Research Article

Graphene oxide-crowned poly(acrylonitrile)/sulfur as a lithium–sulfur battery cathode: performance and characterization

K. Krishnaveni[1] · R. Subadevi[1] · M. Sivakumar[1]

Received: 7 August 2019 / Accepted: 19 March 2020 / Published online: 27 March 2020

Abstract
Polyacrylonitrile (PAN), and graphene oxide (GO), as conductive constituents, were made into a PAN/S/GO composite with sulfur by a solution processing technique. Morphological examination showed that the sulfur and PAN in the composite were wrapped by highly conducting wrinkled layers of GO, aiding in higher utilization of the active mass. The composite exhibited good cycling stability. The first-cycle capacity obtained with PAN/S/GO was 1402 mAh g^{-1} at 0.1 C rate with a Coulombic efficiency of 99%; furthermore, it delivered a capacity of 1096 mAh g^{-1} in the 50th cycle, which was higher than that of and S/GO composites. The improved performance is attributed to the adsorptive properties of GO as well as surface functional groups in GO, which aid in confining polysulfide species within the cathode architecture.

Keywords Lithium–sulfur battery · Solution processing · Sulfur cathode · Polyacrylonitrile · Graphene oxide · Dimethyl sulfoxide

1 Introduction

As portable devices begin to dominate our lives, the demand for high-energy rechargeable batteries is facing an exponential increase [1–4]. Today's lithium-ion batteries (LIBs) based on graphite and $LiCoO_2$/$LiFePO_4$, with limited capacities (100–200 mAh g^{-1}), cannot meet the energy requirements of emerging devices and new applications [5]. Therefore, substantial attention has been devoted towards alternative rechargeable battery systems with considerably higher energy and power densities.

The lithium–sulfur (Li–S) battery system is among candidates that are being considered. As a cathode-active material, sulfur has a theoretical specific capacity of 1675 mAh g^{-1}, which translates to a theoretical energy density of 2600 Wh kg^{-1} (about seven times larger than those of the current LIBs, ~ 387 Wh kg^{-1}). Sulfur also presents other advantages such as non-toxicity, low cost and abundance [6, 7]. However, two disadvantages stand in the way of realizing its full potential in Li–S batteries. First, the poor electrical/ionic conductivity of the active elemental sulfur and the discharge product (Li_2S/Li_2S_2) severely hinders the full capacity utilization of the electrode [8]. Second, dissolution of intermediate long-chain polysulfides into the electrolyte and their shuttle between the cathode and the anode leads to fast capacity degradation and low coulombic efficiency [9]. The insoluble and insulating Li_2S/Li_2S_2 on the surface of electrodes renders the electrodes electrochemically inactive [7]. One of the most popular approaches to resolve these issues is to encapsulate sulfur in an electrically conductive matrix, which enhances the electrical conductivity of the cathode and prevents the dissolution of high-order polysulfides [10, 11]. Various conducting polymers such as poly acrylonitrile (PAN), carbonaceous materials and graphene oxide (GO) have been examined for this purpose.

As the highly insulated material ($\sigma = 10^{-30}$ S/cm), the size of sulfur could largely influence its electrochemical

✉ M. Sivakumar, susiva73@yahoo.co.in | [1]Energy Materials Laboratory, Department of Physics, Science Block, Alagappa University, Karaikudi, Tamil Nadu 630003, India.

performance [12–15]. One way to control the mean size of particles is to control the nucleation rate and supply rate of precursor solute, where the temperature could be an influence factor. During the nucleation stage, the functional groups on GO could facilitate the heterogeneous nucleation of sulfur on the surface of GO nano sheets. Moreover, the low ambient temperatures of preparation could help prevent sulfur agglomeration [16]. Introduction of sulfur in the sulfur cathode composite can conveniently be controlled by low-cost and efficient solution-based processes. Kaiser et al. reported that a large amount of active sulfur loading in sulfur based materials with the help of conventional capillary deposition method [6, 8, 10, 15]. As a constituent of the composite, PAN helps in chemically bonding sulfur to the polymer and can help suppress polysulfide shuttling. However, the limited electrical conductivity of PAN ($\approx 1.51 \times 10^{-11}$ S/cm) lowers capacity retention and rate performance.

In this study, a PAN/S/GO hybrid composite was prepared by a solution processing technique. The sulfur particles were found to be evenly distributed over the GO and interconnected by PAN, which led to short Li^+ diffusion distances and provided rapid ion transport pathways. The PAN/S/GO composite showed an initial discharge capacity of 1402 mAh g^{-1} at 0.1 C. The performance of the composite was compared with that of a GO-wrapped S binary composite (S/GO).

2 Experimental

Sulfur (Alfa Aesar, 100 mesh, 99.5%). and PAN (Sigma–Aldrich, = 1, 50,000, mean particle size 50 µm). were mixed in 4:1 weight ratio, and dispersed in DMSO (Merck). The dispersion was stirred with a weighed amount of GO. The excess solvent was then removed by repeated washing with ethanol and water. The resulting mass was then dried in a vacuum oven. S/GO was also prepared for comparison by a similar method. The GO for this study was prepared by a modified Hummers method [17]. Figure 1 shows the illustration of the preparation of PAN/S/GO composite.

The composites were made into electrodes by a slurry coating method. A slurry containing 70 wt% of the composite, 20 wt% Super P conducting carbon (Timcal) and 10 wt% poly(vinylidene fluoride) binder (Sigma–Aldrich) in *N*-methyl pyrrolidone (Sigma–Aldrich) was coated on aluminum foil current collector. Coin cells of the 2032 configuration (Hohsen) were assembled with lithium metal (Cyprus Foote Mineral) as anode, Celgard 2400 separator and the composite as the cathode. The coin cells were assembled in an MBraun (G-120B) glove box. A 1 M solution of lithium *bis* (trifluoromethane) sulfonamide (Sigma–Aldrich) with 0.05 M $LiNO_3$ (Sigma–Aldrich) in a 1:1 (v/v) mixture of dioxolane (Merck) and dimethyl ether (Merck) was used as the electrolyte. The CR2032 coin cells

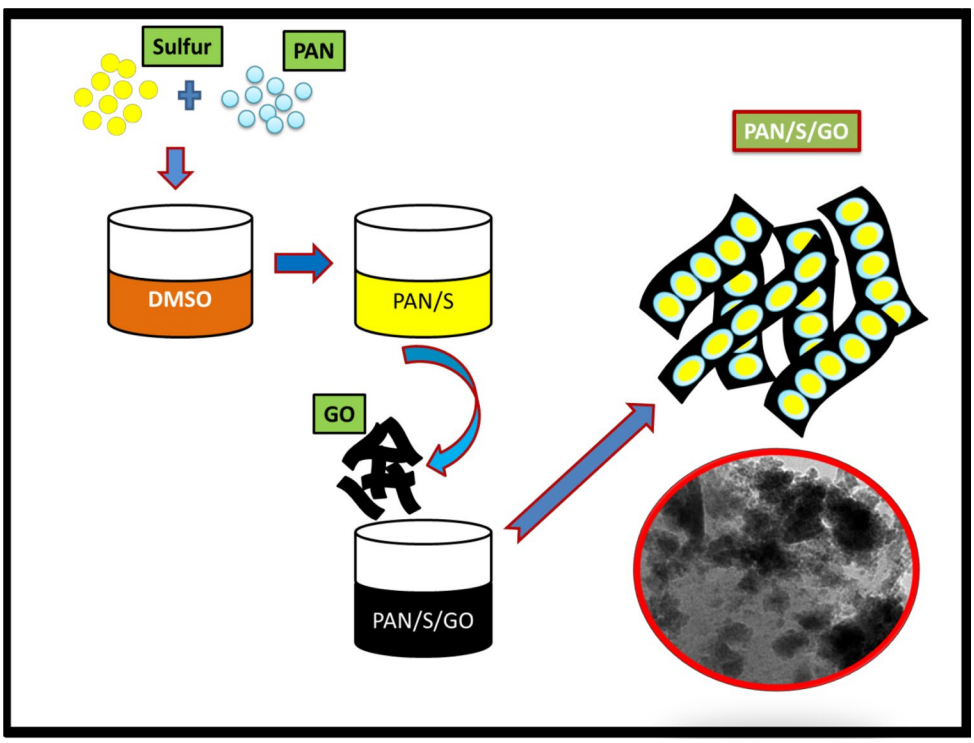

Fig. 1 Shows the illustration of the preparation of PAN/S/GO composite

were assembled with S/GO and PAN/S/GO with areal sulfur loading of 1.8 mg cm^{-2} and 2.4 mg cm^{-2} and lithium metal foil with 0.25 mL electrolyte contained 0.7 M lithium *bis*-trifluoromethane sulfonamide (LiTFSi) (TCI) and 0.05 M $LiNO_3$ (TCI) dissolved in a 1:1 (v/v) mixture of 1,2-dimethoxyethane (Sigma-Aldrich) and 1,3-dioxolane (Sigma-Aldrich) in an argon filled glove box.

2.1 Characterization

Crystal structural features were examined by X-ray diffraction (PANalytical X'pert Pro diffractometer) between scattering angles of 10° and 70° with nickel-filtered Cu K_α radiation. Raman spectroscopic measurements were performed between wavenumbers 100 and 2000 cm^{-1} with a laser radiation wavelength of 632.8 nm (SEKI Focal; He–Ne laser). The surface morphologies of the composites were studied by scanning electron microscopy (FEG, Quanta 250) and transmission electron microscopy (FEI Tecnai 20 G2). Bruanuer–Emmett–Teller surface area measurements were carried out on a Micromeritics ASAP 2010 surface area analyzer. Elemental analysis of the composite was performed by a Perkin-Elmer CHNS 2000 elemental analyzer. X-ray photoelectron spectroscopy (XPS) was carried out on an ESCALAB 250XI X-ray photoelectron spectrometer (Thermo Scientific) with Al KαX-ray source which was performed to analyze the elemental composition of the samples. Cyclic voltammetric studies were run with the coin cells on a Solartron Analytical 1470 E cell test system at a scan rate of 0.1 mV/s between 3.000 and 1.600 V. Galvanostatic charge/discharge profiles were recorded on a multi-channel computerized battery cycler (Arbin, BT 2000) at a 0.1 C rate between 3.000 and 1.600 V at room temperature. The electrochemical impedance spectroscopy (EIS) measurements were carried out (Biologic, France) before cycling of the composite materials.

3 Results and discussion

3.1 Structure and morphology

The XRD patterns of elemental sulfur, PAN, GO and the PAN/S/GO composite are presented in Fig. 1. All the diffraction peaks of elemental sulfur match with those of the standard JCPDS card no. 77-0145, and are index able to

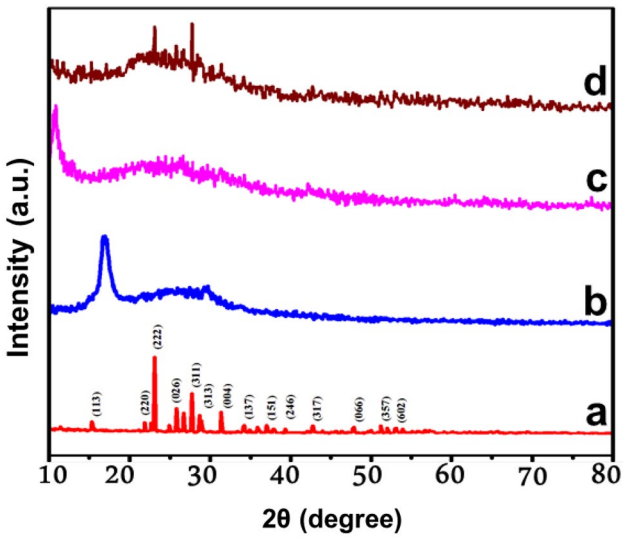

Fig. 2 X-ray diffraction patterns of sulfur; PAN; GO; and PAN/S/GO composite

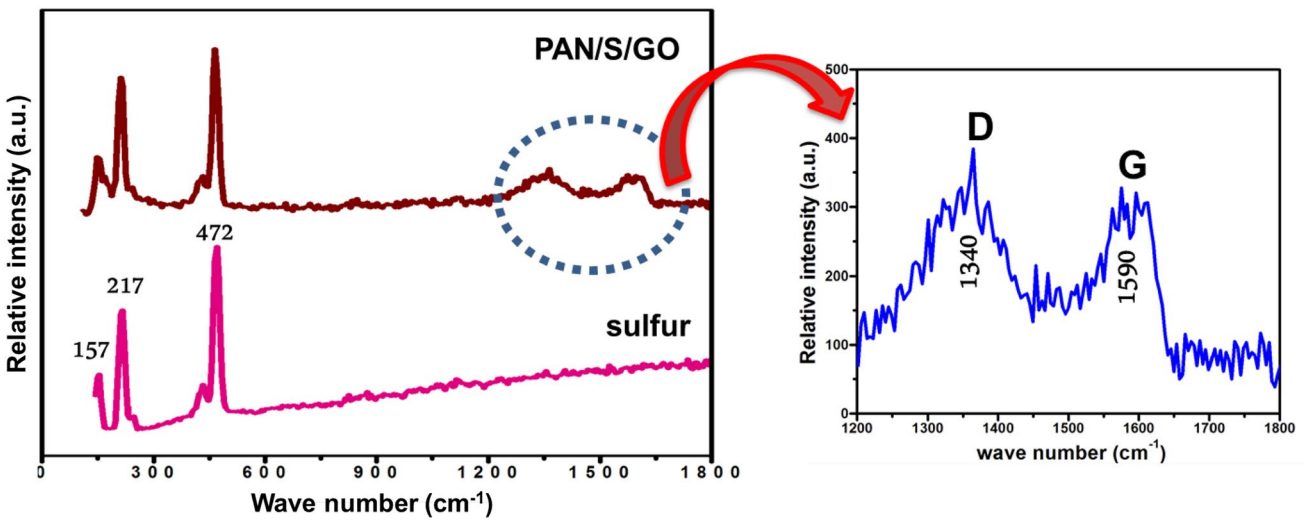

Fig. 3 RAMAN images of the Sulfur and the composite PAN/S/GO

the orthorhombic α-phase of sulfur with space group F_{ddd} (Fig. 1a). The XRD pattern of the pristine PAN has a major peak at a 2θ value of 17°, corresponding to the (110) plane of crystalline PAN (Fig. 1b) [18]. The diffraction pattern of GO show a peak at a 2θ value of 10.5°, corresponding to the (011) plane (Fig. 1c). However, the peaks corresponding to PAN are not discernible in the patterns of the composites, suggesting a definite interaction between sulfur and the polymer. Additionally, the sulfur peaks in the composites appear rather suppressed as they merge with the broad amorphous peaks of GO and PAN. These results indicate a close link in between sulfur, PAN and GO which leads a good cycling process.

Figure 2 shows typical Raman spectra of S and the PAN/S/GO composite. The Raman spectrum of sulfur shows a characteristic peak below 500 cm^{-1} that originates from the *A*1 symmetry mode of the S–S bond (Fig. 3) [19]. The spectrum of GO in the ternary composite elaborates into two peaks at1590 and 1340 cm^{-1}, known respectively as the G (graphitic) and D (disordered) bands (inset). The G band is ascribed to the Raman active E_{2g} in-plane vibration mode and the D band to the A_{1g} mode, similar to the in-plane breathing vibration type due to the presence of disordered areas [20, 21].

The integral intensity ratio (I_D/I_G) is a measure of the degree of graphitization and defects in the GO. The I_D/I_G

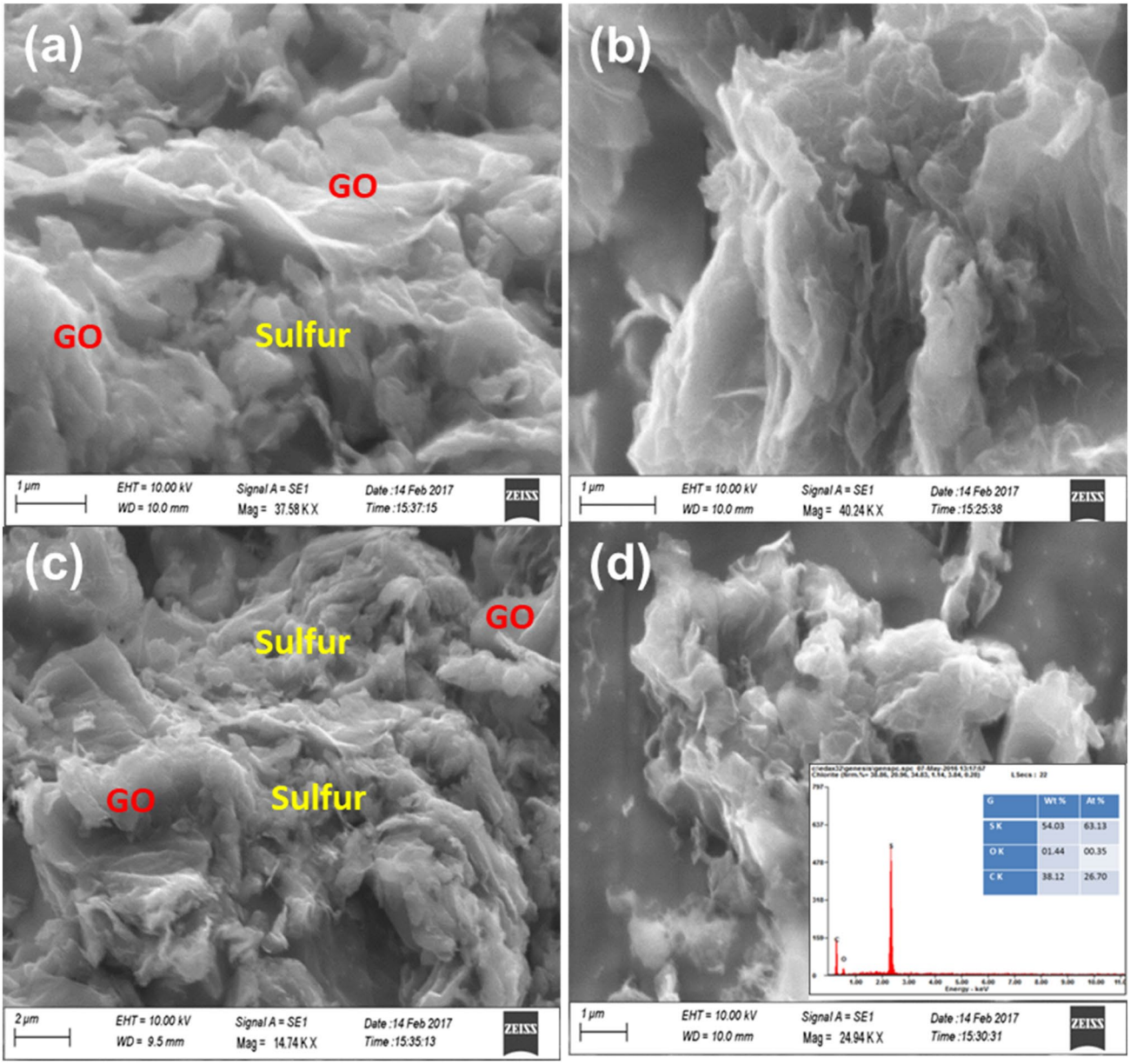

Fig. 4 **a**–**d** SEM image of the ternary PAN/S/GO composite (inset) EDX analysis

of PAN/S/GO is 1.1, suggesting that the GO in the sample has a high degree of defects, which can offer additional energetic sites to facilitate diffusion of Li ions [22]. The Raman spectral results indicate a uniform distribution of sulfur particles in the composite, consistent with our XRD analysis.

SEM images (Fig. 4) of the composite illustrate that the solution processed sulfur particles securely cover the wrinkled GO sheets. This ensures close interaction between the GO and PAN/S, an attribute that results in electron pathways for electrochemical reactions as well as good containment of sulfur in the composite and retention of polysulfides in the matrix. As a dispersant for the preparation of the nano composite, DMSO is advantageous in limiting agglomeration of sulfur nanoparticles. The wrappings by GO sheets help in accommodating lithium polysulfides as well as suppressing volume expansion of the electrode during cycling. This structure could offer an effective

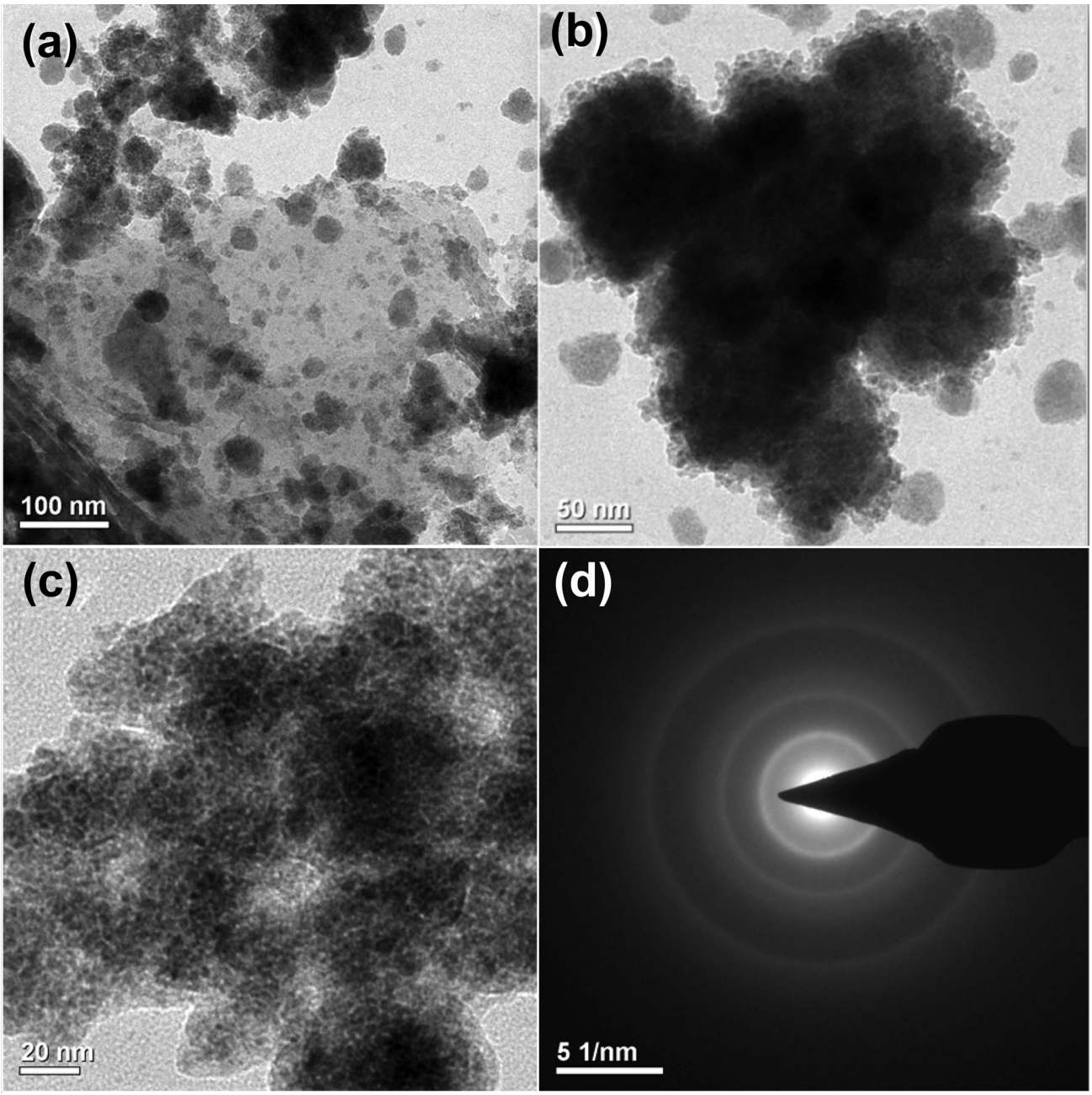

Fig. 5 TEM image of the **a**–**d** ternary PAN/S/GO composite

contact sites for the conductive additives and the active sulfur, which will result in good electrical conductivity.

HRTEM images (Fig. 5a–d) indicate that the treated surfaces have fewer pores and a suitable coating to prevent polysulfide dissolution. The PAN/S/GO nano composite can provide a conductive network and facilitate faster Li+ diffusion in the electrode, resulting in high active material utilization and in sustaining high-rate performance. Moreover, it can be seen from Fig. 5d that the primary PAN/S nanoparticles in the composite has a rather uniform layer of sulfur. The SAED pattern (Fig. 5c inset) suggests the amorphous nature of the sulfur obtained by the solution processing technique. From morphological studies, it can be concluded that the various functional groups of GO, which could hold the sulfur/PAN firmly and well avert the dissolution of polysulfides and diffusion into the electrolyte.

As shown in Fig. 6a, there is a histrionic decrease in the hysteresis loop area of the PAN/S/GO ratifies clearly the loading of sulfur into the GO host. The elemental composition of the PAN/S/GO composite, as determined by CHNS elemental analysis is presented in Table 1. It is seen that the sulfur loading is 54% and is consistent with our EDX analysis.

X-ray photoelectron spectroscopy (XPS) was conducted to study the chemistry of the PAN/S/GO. The high resolution S2*p* peak (Fig. 7a) was fitted to four peaks at binding energies of 162.8 eV, 163.9 eV, 164.7 eV, and 168.5 eV, respectively. Two peaks located at 162.8 and 163.9 eV correspond to the S–S bonds in S_8. The broad peak at 164.7 eV and 168.5 eV is assigned to the C–S and S–O bonds respectively. The spectrum of O1*s* could be divided into two single peaks with binding energies of 531.1 and 532.1 which can be attributed to the oxygen bonds of C–OH and C–O,

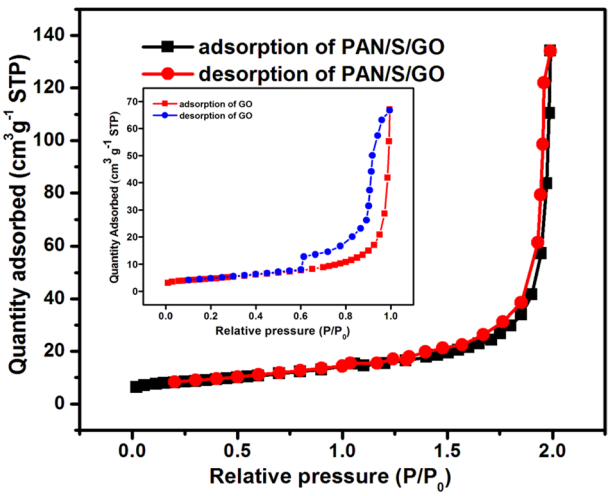

Fig. 6 Nitrogen sorption isotherms of GO and PAN/S/GO composite

Table 1 CHNS elemental composition of the ternary composite

Sample	Weight (mg)	C (mol%)	N (mol%)	S (mol%)	H (mol%)
PAN S/GO	5.0600	39.23	8.217	54.33	0.451

respectively. The high resolution XPS N1*s* spectra for S/PAN/KC sample reveal the presence of two different bands, corresponding to pyridinic-N (~ 398 eV), and pyrrolic-N (~ 399 eV) respectively. The high resolution N1*s* spectra and its deconvolution suggest that N atoms exist as pyridinic (398.8 eV) and pyrrolic (400.2 eV) groups. In the C1*s* spectra, the peaks at can be ascribed to C–O and C–N groups respectively 286.5 eV and 285.4 eV [23].

3.2 Electrochemical properties

Figure 8a shows the CV profile of PAN/S/GO composite cathode between 1.5 and 3 V versus Li +/Li for first cycle at a scan rate of 0.1 mV s^{-1}.In the cathodic reduction process, the peak at 2.3 and 1.9 V can be assigned to the reduction of element sulfur (S_8) to soluble lithium polysulfides (Li_2Sn, $4 \le n \le 8$) and further conversion of these lithium polysulfides to insoluble Li_2S_2 and Li_2S, respectively [24]. Moreover, there are no impure peaks in the curves which exhibit that PAN is stable in the electrode. The oxidation peak at around 2.45 V corresponds to the transformation of Li_2S_2 and Li_2S to Li_2S_8 [25]. The peaks with a shoulder are seen in the CV curves, which usually appear in those sulfur composites with confined structures [26]. The CV results show that the dual structure facilitates preventing polysulfides from dissolving into the electrolyte, owing to the good adsorption performance of GO sheets and PAN.

The charge–discharge curves of S/GO and PAN/S/GO composites at 0.1C rate are shown in Fig. 8b and c. The PAN/S/GO and S/GO composite deliver the initial discharge capacity of 1402 mAh g^{-1} and 937 mAh g^{-1} respectively. Zhang et al. [27] showed that the S/GO ball milled-mixture deliver initial capacity of 927 mAh g^{-1} at 0.1 C. Comparing the S/GO ball milled composite, the solution processed S/GO composite exhibits good electrochemical performance. Moreover, PAN matrix works as secure and stable back bone to form the conducting network in between GO and sulfur particle which leads a good electrochemical performance of the as prepared cathode. The charge- discharge profiles at the 50th cycle of the S/GO and PAN/S/GO composites presented in Fig. 8b and c, confirm that PAN remarkably improves the electrochemical performance of PAN/S/GO. This electrochemical kinetics could be beneficial for utilization of active material. Figure 8d shows the cycling performance of the PAN/S/GO and S/GO composite electrodes at 0.1 C. After 50th cycle

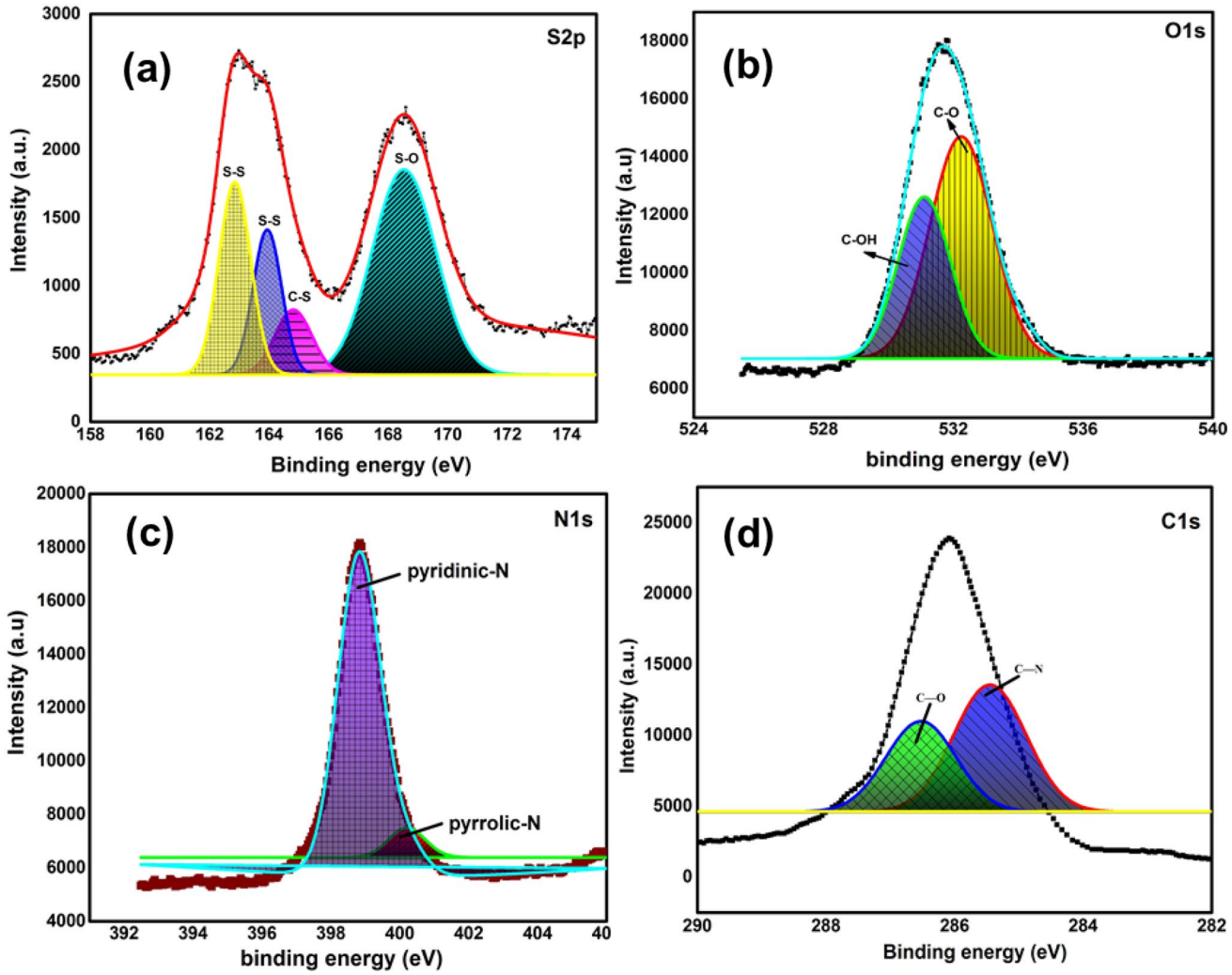

Fig. 7 XPS spectra of PAN/S/GO composite **a** S2*p* **b** O1*s* **c** N1*s* **d** C1*s*

the discharge capacity of 812 mAh g^{-1} remained with the Coulombic efficiency of 95% in the S/GO composite. The Coulombic efficiency of the PAN/S/GO composite in the first cycle is computed to be 99% in comparison to 97% after 65th cycle, indicating reliable stability.

In comparison with S/GO, the PAN/S/GO composite exhibits remarkably enhanced performance, which could be attributed to the very well distribution of sulfur within the polymer matrix [28]. In addition to that the solubility of graphene oxide in DMSO solvents allows it to be uniformly deposited onto sulfur in the form of networks with the support of PAN which creates it possibly suitable for enhancing electrochemical performance of the PAN/S/GO composite. To further investigate the electrochemical properties of the PAN/S/GO composite, a rate performance study was carried out as shown in Fig. 9a. Initial capacities of 1195, 994 and 659 mAh g^{-1} was obtained at rates of 0.2 C, 0.5 C and 1 C respectively. The cell delivers a reversible capacity of 1096 mAh g^{-1} at 0.2 C, confirming a high reversibility and rate capability of the PAN/S/GO composite. The PAN matrix can not only accommodate the mechanical stresses induced by volume changes of the cathode at repeated cycles, but can also facilitate the ions transportation during cycling, leading to efficient cycling performance and rate capability [22]. The upgraded electrochemical kinetics of PAN/S/GO is supported by electrochemical impedance spectroscopy (EIS) measurements (Fig. 9b). Thus, PAN/S/GO possesses the lowest charge transfer resistance, which is interrelated to the enriched interfacial affinity between PAN/S/GO and polysulfide as well as high electrical conductivity of PAN/S/GO [29, 30].

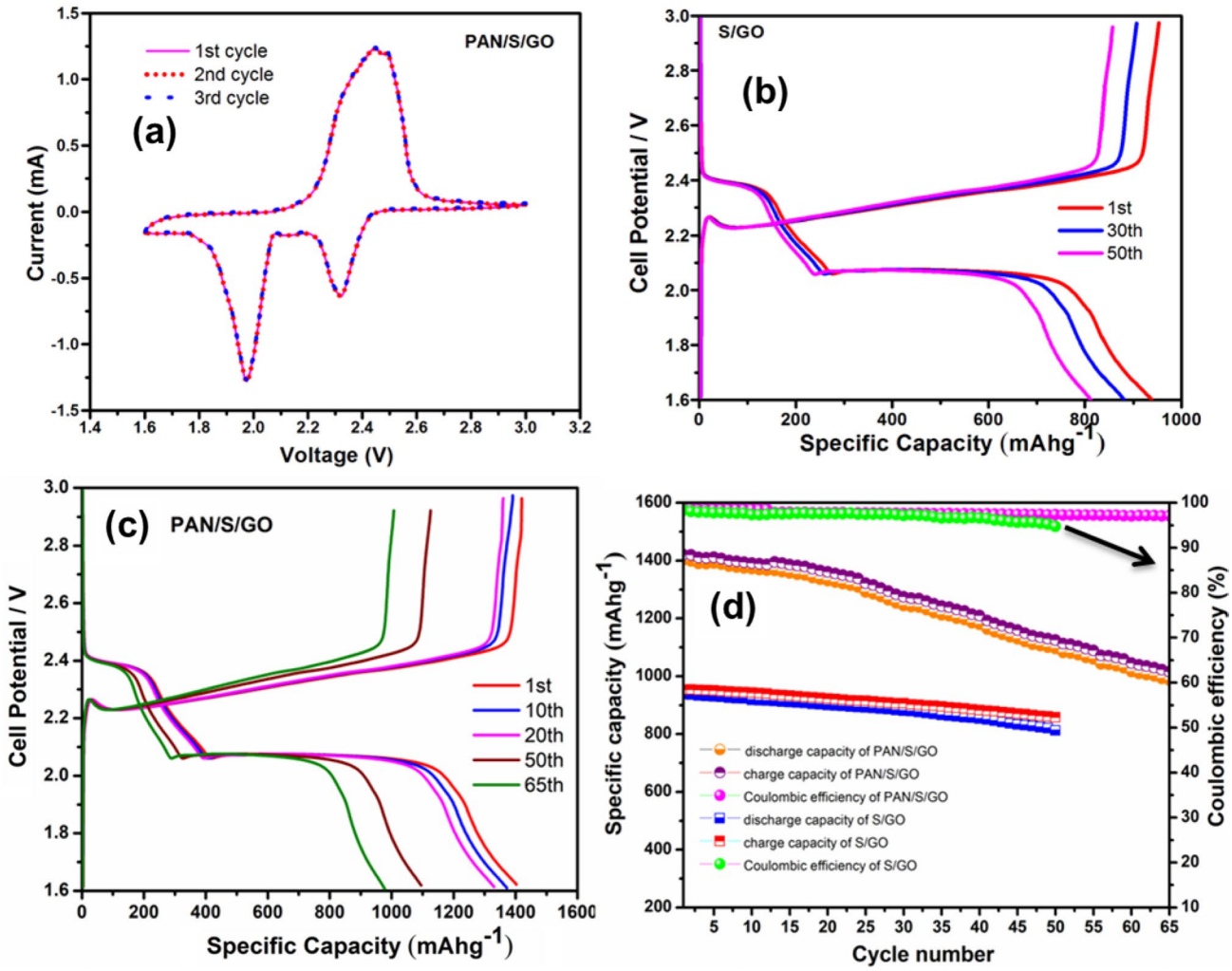

Fig. 8 **a** Cyclic voltammograms of the PAN/S/GO composite for first three cycles **b** discharge/charge voltage profiles of S/GO **c** specific discharge capacities of PAN/S/GO **d** cycling performance of S/GO and PAN/S/GO composites

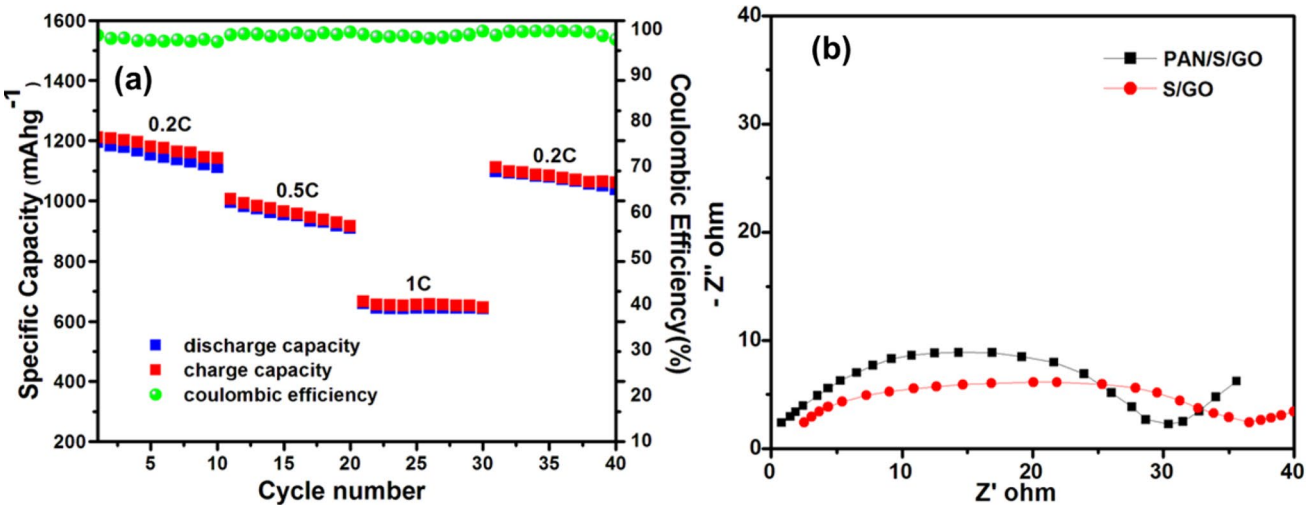

Fig. 9 **a** C rate performance of PAN/S/GO composite **b** Nyquist plots before cycling for S/GO and PAN/S/GO

4 Conclusion

A Polyacrylonitrile/Sulfur/Graphene Oxide composite was prepared by a solution processing technique. The ternary composite delivers an initial discharge capacity of 1402 mAh g^{-1} at C/10 rate. The functional group on the GO and the polymer PAN in the composite help maintain not only suppress the shuttling mechanism but also supports the composite to accommodate the volume changes of sulfur during cycling process. The sulfur particles were evenly distributed over the GO through solution processing technique and were interconnected by PAN, which leaded to short Li^+ diffusion distances and provided rapid ion transport pathways. The cell delivers a reversible capacity of 1096 mAh g^{-1} at 0.2 C, confirming a high reversibility and rate capability of the PAN/S/GO composite.

Acknowledgements All the authors from Alagappa University acknowledge the financial support by DST-SERB, New Delhi under the Physical sciences, Grant sanctioned vide EMR/2016/006302. Also, all the authors gratefully acknowledge for extending the analytical facilities in the Department of Physics, Alagappa University under the PURSE and FIST programme, sponsored by Department of Science and Technology (DST), BSR of University Grants Commission (UGC), New Delhi, Govt. of India and Ministry of Human Resource Development RUSA- Phase 2.0 Grant sanctioned vide Lt.No. F-24-51/2014 U Policy (TNMulti Gen), Dept. of Education, Govt. of India.

Compliance with ethical standards

Conflict of interest We declare that there is no conflict of interest among all authors.

References

1. Armand M, Tarascon JM (2008) Building better batteries. Nature 451:652–657
2. Whittingham MS (2004) Lithium batteries and cathode materials. Chem Rev 104:4271–4301
3. Scrosati B, Hassoun J, Sun YK (2011) Lithium-ion batteries. A look into the future. Energy Environ Sci 4:3287–3295
4. Bruce PG, Freunberger SA, Hardwick LJ, Tarascon JM (2012) Li-O_2 and Li-S batteries with high energy storage. Nat Mater 11:19–29
5. Sivakumar M, Muruganantham R, Subadevi R (2015) Investigations on rate performance of polyol technique developed $LiFePO_4/CeO_2$ composite materials for rechargeable lithium batteries. RSC Adv. https://doi.org/10.1039/C5RA12418B
6. Li F, Kaiser MR, Ma J, Guo Z, Liu H, Wang J (2018) Free-standing sulfur-polypyrrole cathode in conjunction with polypyrrole-coated separator for flexible Li-S batteries. Energy Storage Mater 13:312–322
7. Ji XL, Nazar LF (2010) Advances in Li–S batteries. J Mater Chem 20:9821–9826
8. Kaiser MR, Liang X, Liu HK, Dou SX, Wang JZ (2016) A methodical approach for fabrication of binder-free Li_2S-C composite cathode with high loading of active material for Li-S battery. Carbon 103:163–171
9. Cao Y, Li X, Aksay I, Lemmon J, Nie Z, Yang Z, Liu J (2011) Sandwich-type functionalized graphene sheet-sulfur nanocomposite for rechargeable lithium batteries. Phys Chem Chem Phys 13:7660–7665
10. Kaiser MR, Han Z, Wang J (2019) Electro-polymerized polypyrrole film for fabrication of flexible and slurry-free polypyrrole-sulfur-polypyrrole sandwich electrode for the lithium-sulfur battery. J Power Sour 437:226925
11. Zheng GY, Yang Y, Cha JJ, Hong SS, Cui Y (2011) Hollow carbon nanofiber-encapsulated sulfur cathodes for high specific capacity rechargeable lithium batteries. Nano Lett 11:4462–4467
12. Moon S, Jung YH, Kim DK (2015) Enhanced electrochemical performance of a crosslinked polyaniline coated graphene oxide-sulfur composite for rechargeable lithium-sulfur batteries. J Power Sour 294:386–392
13. Fawaz W, Mosavati N, Abdelhamid E, Ng KS (2019) Synthesis of activated carbons derived from avocado shells as cathode materials for lithium–sulfur batteries. SN Appl Sci 1(4):289
14. Zhu Y, Zhao W, Ye X (2019) Supercritical CO_2-assisted fabrication of CeO_2 decorated porous carbon/sulfur composites for high-performance lithium sulfur batteries. SN Appl Sci 1(5):471
15. Kaiser MR, Han Z, Liang J, Dou SX, Wang J (2019) Lithium sulfide-based cathode for lithium-ion/sulfur battery: recent progress and challenges. Energy Storage Mater 19:1–15
16. Li H, Yang X, Wang X, Liu M, Ye F, Wang J, Qiu Y, Li W, Zhang Y (2015) Dense integration of graphene and sulfur via the soft approach for compact lithium/sulfur battery cathode. Nano Energy 12:468–475
17. Stankovich S, Dikin DA, Piner RD, Kohlhaas KA, Kleinhammes A, Jia Y (2007) Synthesis of graphene-based nanosheets via chemical reduction of exfoliated graphite oxide. Carbon 45:1558–1565
18. Wang J, Yang J, Xie JY, Xu NX (2002) A novel conductive polymer-sulfur composite cathode material for rechargeable lithium batteries. Adv Mater 14:963–965
19. Ward AT (1968) Raman spectroscopy of sulfur, sulfur-selenium, and sulfur-arsenic mixtures. J Phys Chem 72:4133–4139
20. Seo DH, Rider AE, Han ZJ, Kumar S, Ostrikov KK (2013) Plasma break-down and re-build: same functional vertical graphenes from diverse natural precursors. Adv Mater 25:5638–5642
21. Liang X, Wen Z, Liu Y, Wu M, Jin J, Zhang H, Wu X (2011) Improved cycling performances of lithium sulfur batteries with LiNO3-modified electrolyte. J Power Sour 196:9839–9843
22. Krishnaveni K, Subadevi R, Radhika G, Premkumar T, Raja M, Liu WR, Sivakumar M (2018) Carbon wrapping effect on sulfur/polyacrylonitrile composite cathode materials for lithium sulfur batteries. J Nanosci Nanotechnol 18(1):121–126
23. Jeon IY, Zhang S, Zhang L, Choi HJ, Seo JM, Xia Z, Dai L, Baek JB (2013) Edge-selectively sulfurized graphene nanoplatelets as efficient metal-free electrocatalysts for oxygen reduction reaction: the electron spin effect. Adv Mater 25:6138–6145
24. Rauh RD, Abraham KM, Pearson GF, Surprenant JK, Brummer SB (1979) A lithium/dissolved sulfur battery with an organic electrolyte. Electrochem Soc 126:523–527
25. Zu C, Manthiram A (2014) Stabilized lithium-metal surface in a polysulfide-rich environment of lithium-sulfur batteries. J Phys Chem Lett 5(15):2522–2527
26. Li LY, Liu X, Zhu K, Tian J, Liu X, Yang K, Shan Z (2015) PEO coated sulfur-carbon composite for high performance lithium-sulfur batteries. J Solid State Electrochem. https://doi.org/10.1007/s10008-015-2961-1
27. Zhang Y, Zhao Y, Bakenov Z (2014) A simple approach to synthesis nanosized sulfur/graphene oxide materials for high performance lithium- sulfur batteries. Ionics 20:1047–1050
28. Jeddi K, Sarikhani K, Qazvini NT, Chen P (2014) Stabilizing lithium-sulfur batteries by a composite polymer electrolyte containing mesoporous silica particles. J Power Sour 245:656–662
29. Wang C, Su K, Wan W, Guo H, Zhou H, Chen J, Zhang X, Huang Y (2014) High sulfur loading composite wrapped by 3D

nitrogen-doped graphene as a cathode material for lithium–sulfur batteries. J Mater Chem A 2:5018–5023
30. Sun Z, Zhang J, Yin L, Hu G, Fang R, Cheng HM, Li F (2017) Conductive porous vanadium nitride/graphene composite as chemical anchor of polysulfides for lithium-sulfur batteries. Nat Commun 8:14627